High-spin states of the $N = 82$ isotones ^{136}Xe, ^{137}Cs, and ^{138}Ba: Monopole-driven competition of neutron core excitations with two-proton excitations to the $h_{11/2}$ high-j orbit

Hua Jin (金华) ●,[1,2,3] Shigeru Tazaki (田崎茂) ●,[2] Kazunari Kaneko (金子和也),[4]
Han-Kui Wang (王韩奎),[5] and Yang Sun (孙扬)[3,6,*]

[1]*School of Arts and Sciences, Shanghai Dianji University, Shanghai 201306, China*
[2]*Department of Applied Physics, Fukuoka University, Fukuoka 814-0180, Japan*
[3]*Key Laboratory of High Precision Nuclear Spectroscopy, Institute of Modern Physics, Chinese Academy of Sciences, Lanzhou 730000, China*
[4]*Department of Physics, Kyushu Sangyo University, Fukuoka 813-8503, Japan*
[5]*School of Physics and Mechanical and Electrical Engineering, Zhoukou Normal University, Henan 466000, China*
[6]*School of Physics and Astronomy, Shanghai Jiao Tong University, Shanghai 200240, China*

It is known that the monopole effect in shell-model calculations can influence single-particle states dynamically, resulting in novel shell evolution near the ground state. We show that a monopole-driven competition between different excitation modes can occur in the high-lying, high-spin states in nuclei above ^{132}Sn. Stimulated by the recent high-spin data, we extend large-scale shell-model calculations with the effective interaction determined in our previous work [Phys. Rev. C **84**, 044324 (2011)] to study the heavier $N = 82$ isotones ^{136}Xe, ^{137}Cs, and ^{138}Ba. With inclusion of configurations for neutron core excitation across the $N = 82$ shell gap, we treat simultaneously two kinds of excitation modes for the high-spin states, namely, those from multiproton coupling within the valence-proton space and from neutron core excitation to the upper orbits above the $N = 82$ shell gap. Based on a good reproduction of the experimental data, we discuss the competition mechanism by analyzing the monopole effect in the effective single-particle energies.

I. INTRODUCTION

The structural evolution of the single-particle states near the doubly closed-shell nucleus ^{132}Sn has long been a study focus [1,2], which has motivated a lot of experimental work, particularly in recent years [3–16]. For this neutron-rich mass region, investigations have been carried out aiming at understanding the magic nature of ^{132}Sn [3,4], the nucleon-nucleon interactions [5–7], and the shell evolution when particles and/or holes are added to ^{132}Sn [8–11]. Furthermore, as the astrophysical rapid neutron-capture process (r process) proceeds through the ^{132}Sn region, the study is important also for elucidating questions on the r-process nucleosynthesis [12–16]. Specifically, the shell evolution below ^{132}Sn has been extensively investigated from both experimental and theoretical points of view [8–11,17–20]. Along the $N = 82$ line, one recent interest is to extend the discussion to the $N = 82$ isotones beyond $Z = 50$.

The $N = 82$ isotone ^{136}Xe is a candidate in the search for neutrinoless double-β decay ($0\nu\beta\beta$) (see the recent report in Ref. [21]). Comprehensive structural information provides crucial tests of the nuclear structure models used in calculating the nuclear matrix element for $0\nu\beta\beta$ and in extracting the neutrino mass, if this exotic decay process is observed. As ^{136}Xe is a closed-neutron-shell nucleus with four protons in

excess of the $Z = 50$ closed shell, it is usually expected that it should contain low-lying excitations with $(\pi g_{7/2})^2$ or $(\pi d_{5/2})^2$ configurations and combinations of them. Indeed, candidates for such states have been experimentally identified [22,23].

On the other hand, during the past two decades, high-spin data at high excitations in some $N = 82$ and 83 isotones beyond ^{132}Sn have become available from the study of different reaction products by using large γ-ray detector arrays [24–32]. Of special interest is the core-excited states across the neutron $N = 82$ shell gap. Such cross-shell excitations provide a unique access to the size of the $N = 82$ shell gap and can thus enhance our understanding of the shell variation when particles are added to ^{132}Sn. In Ref. [32], high-spin states of five heavier $N = 82$ isotones ^{136}Xe, ^{137}Cs, ^{138}Ba, ^{139}La, and ^{140}Ce have been updated by the experiment of two fusion-fission reactions.

On the theoretical side, shell models based on the spherical basis are usually the theoretical tool for the description of nuclei near the shell closures. In the past, some of these core-excited states were well reproduced by the empirical interactions with simple configurations [26–28]. For the new data [32], the empirical interaction and later the SN100PN interaction [33] were employed to explain the high-spin states at high excitations. However, these calculations were restricted within the proton valence-particle space of the 50–82 shell. Although for some high-spin levels in ^{136}Xe, ^{137}Cs, and ^{138}Ba, the authors in both Refs. [32,33] speculated that their structures could involve neutron core excitations across the

$N = 82$ shell gap, no actual calculations were given due to the limitation in their shell-model space.

In our earlier work [34], shell-model calculations with a large model space including neutron core-excitation configurations were carried out for the energy levels up to high spins for some $A = 133$–135 nuclei above ^{132}Sn. The calculation employed the extended paring-plus-quadrupole interaction with monopole corrections (EPQQM) and systematically explained both the low-lying and highly-excited states of the $N = 82$ isotones ^{133}Sb, ^{134}Te, and ^{135}I and the $N = 83$ isotones ^{133}Sn, ^{134}Sb, and ^{135}Te. Later, the EPQQM model with a model space considering both proton and neutron core excitations was successfully applied to study the structure of the hole nuclei [35–37], exploring the evolution of the neutron $N = 82$ closed shell below ^{132}Sn [19,20]. All these works have demonstrated that the EPQQM model is a practical method for the description of core excitations around ^{132}Sn.

The purpose of the present work is to apply the EPQQM model with the same effective interaction determined in Ref. [34] to study the structural variation in the heavier $N = 82$ isotones above ^{132}Sn. Unlike other shell-model studies [32,33], we emphasize the competition of two excitation modes at high spins: the proton excitations within the valence-proton space as discussed in Refs. [32,33] and the neutron core excitations across the $N = 82$ shell gap as introduced in our earlier work. The latter mode was speculated in Refs. [32,33], but has not been quantitatively demonstrated so far. We discuss the important role played by the monopole correction terms in the EPQQM model and show how the effective single-particle energies (ESPEs) change dynamically with particle occupations under the influence of the monopole terms.

The paper is organized as follows. In Sec. II, the EPQQM interaction and the corresponding model space adopted for the present shell-model calculation are briefly outlined. In Sec. III, we discuss the calculated results for the three $N = 82$ isotones ^{136}Xe, ^{137}Cs, and ^{138}Ba and compare them with the available experimental data. The high-spin structures with neutron core excitations are analyzed in detail, and the resulting ESPEs in the presence of the monopole correction terms are discussed in this section. Finally, conclusions are given in Sec. IV.

II. OUTLINE OF THE THEORY

The EPQQM model was originally developed for shell-model calculations in lighter $N \approx Z$ nuclei [38,39]. Later, it was extended to apply to different mass regions [34,40–42]. In recent years, the EPQQM has been successfully applied to the ^{132}Sn mass region [19,20,34–37]. For the nuclei near ^{132}Sn, in which protons and neutrons occupy orbits belonging to different major shells, the EPQQM model has the advantage that it can determine two-body matrix elements (TBMEs) using the separable forces, supplemented with monopole corrections [34]. Thus, to compare with other interactions adopted for the ^{132}Sn region (for example, the realistic effective interactions derived from bare nucleon-nucleon potential [43] or the empirical ones based on fitting experimental data [44]),

the EPQQM interaction in its simple form can treat both the low-lying and cross-shell high excitations on an equal footing.

In the present work, we employ the same EPQQM interaction and the model space introduced in Ref. [34]. In the proton-neutron (pn) representation, the Hamiltonian is written in the separable form as follows:

$$
\begin{aligned}
H &= H_{\text{sp}} + H_{P_0} + H_{P_2} + H_{QQ} + H_{OO} + H_{HH} + H_{\text{mc}} \\
&= \sum_{\alpha,i} \varepsilon_\alpha^i c_{\alpha,i}^\dagger c_{\alpha,i} - \frac{1}{2} \sum_{J=0,2} \sum_{ii'} g_{J,ii'} \sum_M P_{JM,ii'}^\dagger P_{JM,ii'} \\
&\quad - \frac{1}{2} \sum_{\lambda=2,3,4} \sum_{ii'} \frac{\chi_{\lambda,ii'}}{b_0^{2\lambda}} \sum_M : \mathcal{Q}_{\lambda M,ii'}^\dagger \mathcal{Q}_{\lambda M,ii'} : \\
&\quad + \sum_{j_a \leqslant j_b, ii'} k_{mc}(ia, i'b) \sum_{JM} A_{JM}^\dagger(ij_a, i'j_b) A_{JM}(ij_a, i'j_b).
\end{aligned}
\tag{1}
$$

In Eq. (1), the indices i and i' stand for proton (π) and neutron (ν), respectively, and b_0 is the harmonic-oscillator range parameter. The Hamiltonian includes the $J = 0$ and $J = 2$ pairing (P_0 and P_2) terms, the multipole-multipole terms (with multipolarity $\lambda = 2, 3, 4$), and the monopole corrections (H_{mc}). The corresponding interaction strengths $g_{J,ii'}$, $\chi_{2,ii'}$, $\chi_{3,ii'}$, $\chi_{4,ii'}$, and $k_{mc}(ia, i'b)$ were determined (see Ref. [34]) for the nuclei with $Z \geqslant 50$ beyond ^{132}Sn. For the adopted monopole corrections in the calculation, the two attractive terms $k_{mc}(\pi g_{7/2}, \pi h_{11/2}) = -0.15$ and $k_{mc}(\pi g_{7/2}, \nu h_{9/2}) = -0.6$ (both in MeV) are the most relevant ones to the present study, and their effects will be emphasized below.

The ^{116}Sn ($Z = 50$ and $N = 66$) is chosen as the core [34]. The valence nucleons are included in the following model space outside ^{116}Sn: five proton orbits ($0g_{7/2}$, $1d_{5/2}$, $2s_{1/2}$, $1d_{3/2}$, and $0h_{11/2}$), five upper neutron orbits ($1f_{7/2}$, $2p_{3/2}$, $0h_{9/2}$, $2p_{1/2}$, and $1f_{5/2}$), and two lower neutron orbits ($0h_{11/2}$ and $1d_{3/2}$). As ^{116}Sn is not a doubly magic nucleus, the single-particle energies for the present model space, ε_α^i in Eq. (1), cannot be directly obtained from experiment. They should be determined by modifying the experimental single-particle and single-hole energies around ^{132}Sn by considering particle-hole interactions (for details, see Ref. [34]).

Calculations are performed with the J-scheme shell-model code NUSHELLX [45]. For the neutron valence space, only one particle-hole excitation is allowed from each lower orbit to the upper ones across the $N = 82$ shell gap. Except for this restriction in neutron core excitations, no other truncations are necessary with respect to the proton valence space for the $N = 82$ isotones ^{136}Xe and ^{137}Cs. For ^{138}Ba, we fix at least two valence protons to occupy the lowest $\pi g_{7/2}$ orbit. However, for the even heavier isotones ^{139}La and ^{140}Ce, calculations with NUSHELLX in the same model space are not feasible because of the computational limit of the code.

In order to investigate the shell evolution of the $N = 82$ isotones with varying proton numbers, we evaluate ESPEs from the monopole Hamiltonian in the pn representation [46],

$$
H_m = \sum_{a,i} \varepsilon_a^i \hat{n}_{ai} + \sum_{ab,ii'} V_{ab}^{ii'} \frac{\hat{n}_{ai}(\hat{n}_{bi'} - \delta_{ab}\delta_{ii'})}{1 + \delta_{ab}\delta_{ii'}}.
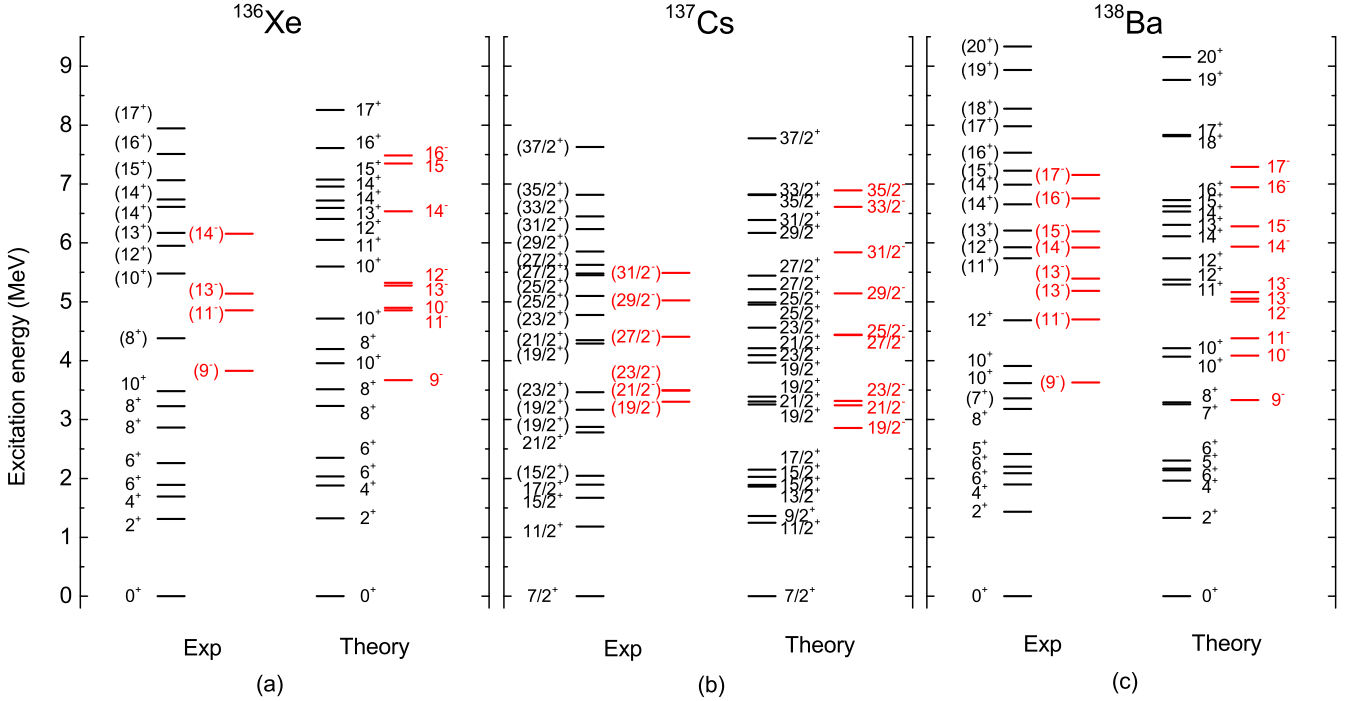\tag{2}
$$

FIG. 1. Calculated energy levels for the $N = 82$ isotones: (a) ^{136}Xe, (b) ^{137}Cs, and (c) ^{138}Ba. The available experimental data, taken from Ref. [32], are shown for comparison. Lines with black (red) color are for positive-parity (negative-parity) states.

In Eq. (2), $\hat{n}_{ai}$ is the particle-number operator and $V_{ab}^{ii'}$ is the monopole component of the two-body interaction [46],

$$V_{ab}^{ii'} = \frac{\sum_J \langle i j_a, i' j_b | V | i j_a, i' j_b \rangle_J (2J+1)[1 + (-1)^J \delta_{ii'} \delta_{ab}]}{(2j_a + 1)(2j_b + 1 - \delta_{ii'} \delta_{ab})},$$

(3)

where $\langle i j_a, i' j_b | V | i j_a, i' j_b \rangle_J$ represents the TBMEs. The ES-PEs are defined as energy differences of the monopole Hamiltonian caused by removing one nucleon from an occupied orbital or adding one nucleon to an unoccupied orbital [46]. It is known that the monopole interaction plays a significant role for the shell evolution because of the monopole shift when valence nucleons occupy certain orbits [47]. It should be noted that the monopole corrections represent the main ingredients of the monopole interaction in our model. Therefore, some monopole corrections, especially those involving the $\pi g_{7/2}$ orbit, will strongly influence the ESPEs and lead to the structural evolution when the occupations on the $\pi g_{7/2}$ orbit are enhanced in the $N = 82$ isotones.

III. RESULTS AND DISCUSSIONS

Large-scale shell-model calculations based on our EPQQM model are performed to describe the overall spectroscopy observed in three $N = 82$ isotones, ^{136}Xe, ^{137}Cs, and ^{138}Ba. In Fig. 1, we show the calculated energy levels and compare them with the updated experimental data of Astier *et al.* [32]. We analyze in detail the structure of the energy levels for both low-lying and high excitation levels. Moreover, we focus the discussion on the monopole-driven effect on the high-spin states and reveal the competition between the

neutron core excitation across the $N = 82$ closed shell and two-proton excitation to the $\pi h_{11/2}$ orbit. Other shell-model calculations [32,33,48] were successfully carried out for the $N = 82$ isotones beyond ^{132}Sn. However, with their limited neutron valence space, the authors could not discuss the neutron core-excited states.

A. Positive-parity states

In this section, we discuss the positive-parity states of these nuclei. The discussion is divided into two subsections, for low-lying states and high-spin states at high excitations.

1. Low-lying states

In the $N = 82$ isotones, the low-lying states correspond to proton excitations, for which the configurations are built within the proton shells ($0g_{7/2}$, $1d_{5/2}$, $2s_{1/2}$, and $1d_{3/2}$). Among the above four orbits, only $0g_{7/2}$ and $1d_{5/2}$ are relevant to the low-lying states. The experimentally observed states have been successfully described by different effective interactions [32,33,48–51]. In our previous work [34], the EPQQM model studied such states of the lighter $N = 82$ isotones ^{134}Te and ^{135}I.

As one can see in Figs. 1(a)–1(c), the experimentally known levels below 5 MeV for the two proton-even isotones ^{136}Xe and ^{138}Ba, and those below 4 MeV for the proton-odd isotone ^{137}Cs, are described reasonably well. The analysis of wave functions suggests that for all the low-lying positive-parity states presented in Fig. 1, the valence protons basically occupy the two orbits, $\pi g_{7/2}$ and $\pi d_{5/2}$. The main configurations of those states correspond to $(\pi g_{7/2})^n$, $(\pi g_{7/2})^{n-1}(\pi d_{5/2})^1$, and $(\pi g_{7/2})^{n-2}(\pi d_{5/2})^2$, or combinations

of them, where n is the number of valence protons. We can simply denote these configurations as $(\pi g_{7/2} \pi d_{5/2})^n$.

γ-ray cascades down to the ground state were observed in the three isotones (see Figs. 1, 6, and 7 in Ref. [32]). Our calculation indicates that these low-lying states are characterized by a mixed nature with different configurations. We take the yrast states, i.e., the assemble of the lowest state for each spin, as examples. For ^{136}Xe, the calculation suggests that the 8_1^+ state has a relatively pure $(\pi g_{7/2})^4$ configuration. The 0_1^+, 2_1^+, 4_1^+, and 6_1^+ states contain some components from $(\pi g_{7/2})^2(\pi d_{5/2})^2$, but have a considerable component of $(\pi g_{7/2})^4$. For ^{138}Ba, all the yrast states up to 12_1^+ have the component of $(\pi g_{7/2})^4(\pi d_{5/2})^2$ except the 10_1^+ state, whose leading configuration is $(\pi g_{7/2})^5(\pi d_{5/2})^1$. However, the $(\pi g_{7/2})^6$ component is also not small in the 0_1^+, 2_1^+, 4_1^+, and 6_1^+ states. Our suggested configurations for ^{136}Xe and ^{138}Ba are basically consistent with the results reported in Ref. [33]. For ^{137}Cs, the calculated yrast states with $7/2_1^+$ to $23/2_1^+$ do not assume any predominant configurations. The $7/2_1^+$, $11/2_1^+$, and $15/2_1^+$ states have a leading configuration of $(\pi g_{7/2})^5$, but with some differences. The $7/2_1^+$ and $11/2_1^+$ states are mixed with a considerable amount of $(\pi g_{7/2})^3(\pi d_{5/2})^2$ component, while this component is small in $15/2_1^+$. The $17/2_1^+$, $19/2_1^+$, and $21/2_1^+$ states belong to the $(\pi g_{7/2})^4(\pi d_{5/2})^1$ multiplet, and $23/2_1^+$ is a member of the $(\pi g_{7/2})^3(\pi d_{5/2})^2$ one. These configurations are consistent with the analysis for the yrast states of ^{137}Cs in Refs. [25,30].

It should be pointed out that there are several low-lying positive-parity states in Fig. 1 that are not reproduced in the correct energy as compared to the experiment. For example, the calculated $19/2_1^+$, $21/2_1^+$ and $23/2_1^+$ states of ^{137}Cs, and the 12_1^+ state of ^{138}Ba, are higher than the observed ones. There are also low-lying states that should be there but have not be experimentally identified. In Fig. 1(b), we predict the missing $9/2_1^+$ and $13/2_1^+$ states at excitation energies of 1.363 and 1.863 MeV, respectively. Their wave functions indicate that they are members of the $(\pi g_{7/2})^4(\pi d_{5/2})^1$ multiplet.

In Table I, we show the calculated electric quadrupole transition probabilities, $B(E2)$, for low-lying states of the three isotones, and compare them, if possible, with the experimental data from Ref. [52]. In the calculation, the standard effective charges $e_\pi = 1.5e$ and $e_\nu = 0.5e$ are employed. Most of the resulting $B(E2)$ values among these low-lying states range from a few W.u. to a few percents of W.u.. In ^{136}Xe, for example, stronger $B(E2)$ transitions following the yrast cascades up to 4_1^+, but at 6^+, the $B(E2)$ strength becomes fragmented due to the existence of two 6^+ states with mixed structures. This feature is experimentally suggested, and supported by the calculation. In ^{138}Ba, The first two $B(E2)$ transitions, $B(E2, 2_1^+ \to 0_1^+)$ and $B(E2, 4_1^+ \to 2_1^+)$, exhibit a difference in nearly two orders of magnitude, which is correctly described by the calculation. A similar situation is seen also in the odd-mass ^{137}Cs. Significant differences are seen for the first two $B(E2)$ transitions in the yrast states. While the large value for $B(E2, 11/2_1^+ \to 7/2_1^+)$ suggests that the structures of the $7/2_1^+$ and $11/2_1^+$ states are similar, the small $B(E2, 15/2_1^+ \to 11/2_1^+)$ means that the structure of $15/2_1^+$ must be different from them. The differences in structure for these three states were discussed before.

TABLE I. Comparison of the calculated and experimental $B(E2)$ values for ^{136}Xe, ^{137}Cs, and ^{138}Ba. The experimental data are taken from Ref. [52].

Nucleus	Transition	$B(E2)$ in (W.u.)	
		Expt.	Theory
^{136}Xe	$2_1^+ \to 0_1^+$	9.7(4)	10.32
	$4_1^+ \to 2_1^+$	1.281(17)	3.00
	$6_1^+ \to 4_1^+$	0.0132(8)	0.17
	$6_2^+ \to 4_1^+$	>0.26	0.89
	$8_1^+ \to 6_1^+$		4.32
	$8_1^+ \to 6_2^+$		0.02
	$8_2^+ \to 6_1^+$		0.29
	$8_2^+ \to 6_2^+$		6.43
	$10_1^+ \to 8_1^+$		0.05
	$10_1^+ \to 8_2^+$		6.86
^{137}Cs	$11/2_1^+ \to 7/2_1^+$		9.12
	$15/2_1^+ \to 11/2_1^+$		0.27
	$17/2_1^+ \to 15/2_1^+$		0.002
	$21/2_1^+ \to 17/2_1^+$		5.62
	$23/2_1^+ \to 21/2_1^+$		0.18
^{138}Ba	$2_1^+ \to 0_1^+$	11.0(4)	12.75
	$4_1^+ \to 2_1^+$	0.2878(15)	0.41
	$6_1^+ \to 4_1^+$	$0.053\binom{+8}{-6}$	0.67
	$6_2^+ \to 4_1^+$	–	0.62
	$8_1^+ \to 6_1^+$	$0.32\binom{+79}{-17}$	5.17
	$8_1^+ \to 6_2^+$	$0.18\binom{+47}{-10}$	3.99
	$10_1^+ \to 8_1^+$	$1.59\binom{+26}{-20}$	4.34
	$10_2^+ \to 8_1^+$	>4.1	3.81
	$12_1^+ \to 10_1^+$	–	1.79
	$12_1^+ \to 10_2^+$	>3.3	6.77

2. High-spin states

While the positive-parity states at low excitations are coupled by the proton $0g_{7/2}$ and $1d_{5/2}$ orbits, proton excitations to the upper $\pi h_{11/2}$ orbit can lead to states with high excitation energies. Because of the coupling to the high-j orbit, these highly excited states are usually also high-spin states. What we want to emphasize is that for the $N = 82$ isotones under discussion, neutron core excitations from the lower $\nu h_{11/2}$ orbit across the $N = 82$ shell gap can also form high-spin, high-energy, positive-parity states. As we now discuss, the two kinds of excitation modes, the neutron cross-shell excitation and the proton excitation to the upper $\pi h_{11/2}$ orbit, may create states at the same energy range that thus compete with each other. The competition picture does not exist in the previous shell-model calculations [32,33] as they dealt with one excitation mode only.

As one can see in Fig. 1(a), the calculated positive-parity levels above 5 MeV in ^{136}Xe are in good agreement with the experimental ones [32], both in energy and in their orders. We thus suggest that the observed high-spin states from (10_2^+) up to (17_1^+) in ^{136}Xe correspond to our calculated 10_3^+, 12_1^+, 13_1^+, 14_1^+, 14_2^+, 15_1^+, 16_1^+, and 17_1^+ states, respectively. In addition,
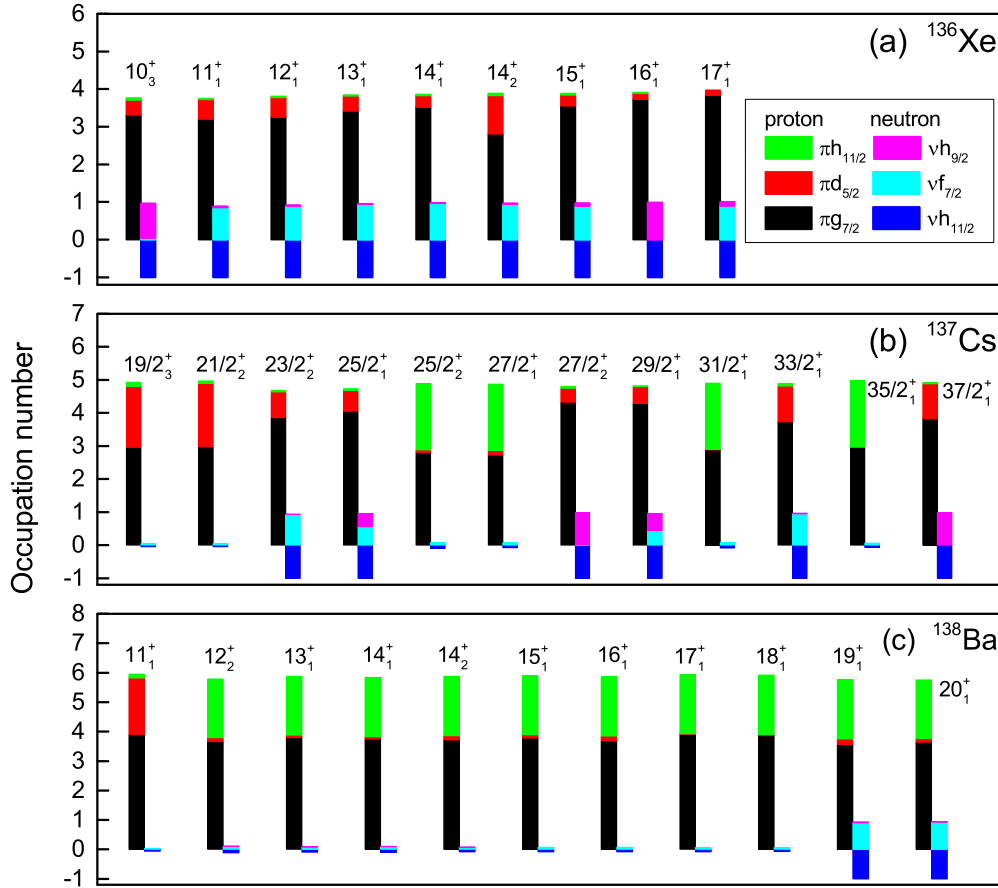
FIG. 2. The occupation numbers of the main orbits involved in configuration for the calculated high-spin states with positive parity in the nuclei (a) ^{136}Xe, (b) ^{137}Cs, and (c) ^{138}Ba. For neutrons, negative occupations mean the hole numbers in the $\nu h_{11/2}$ orbit below the $N = 82$ shell gap. These theoretical states correspond to the calculated energy levels drawn in Figs. 1(a)–1(c).

we predict an unobserved 11_1^+ state at 6.052 MeV. The calculated second 10_2^+ state is a member of the $(\pi g_{7/2})^2(\pi d_{5/2})^2$ multiplet and is lower in energy than the observed (10_2^+) state.

We can further propose structure for these high-spin states. In Fig. 2, we present the theoretical occupation numbers in various orbits for the calculated high-spin states starting from 10_3^+ in Fig. 1(a) for ^{136}Xe, $19/2_3^+$ in Fig. 1(b) for ^{137}Cs, and 11_1^+ in Fig. 1(c) for ^{138}Ba.

In Fig. 2(a) for ^{136}Xe, we find that all the presented nine states contain significant components of neutron excitations across the $N = 82$ shell, while components of proton excitations to the upper $\pi h_{11/2}$ orbit are small. Specifically, most of these states are found to have a leading configuration of $(\pi g_{7/2}\pi d_{5/2})^4(\nu h_{11/2})^{-1}(\nu f_{7/2})^1$, except the 10_3^+ and 16_1^+ states, which take the configuration of $(\pi g_{7/2}\pi d_{5/2})^4(\nu h_{11/2})^{-1}(\nu h_{9/2})^1$. It is interesting to note that these two high-spin states involve the configuration with a neutron cross-shell excitation to the $\nu h_{9/2}$ orbit. As $\nu h_{9/2}$ is the $l = 5$ partner of the $h_{11/2}$ intruder orbit, the energy separation of the two orbits measures directly the size of the neutron $N = 82$ shell gap. We point out that the neutron $h_{9/2}$ occupation is influenced by the monopole correction $k_{mc}(\pi g_{7/2}, \nu h_{9/2})$ in the present EPQQM model [34]. This large attractive term (with the strength of -0.6 Mev) greatly pushes the $\nu h_{9/2}$ orbit

down to be close to $\nu f_{7/2}$, which facilitates neutron cross-shell excitations to $\nu h_{9/2}$. The monopole correction modifies the single-particle states as seen in the calculated ESPEs, which will be discussed later.

Astier *et al.* discussed [32] how their shell-model calculation with the configuration of $(\pi g_{7/2}\pi d_{5/2})^2(\pi h_{11/2})^2$ could not reproduce the experimental data for the high-spin positive-parity states in ^{136}Xe (see Fig. 14(a) of Ref. [32]). This configuration describes the high-energy states as two proton excitations to the upper $\pi h_{11/2}$ orbit. In order to compare excitation energies calculated with different configurations, we plot in Fig. 3(a) the lowest excitation energies calculated with each of the configurations. For comparison, the experimentally observed corresponding states are also shown. As one can see, the calculated energies of the two-proton configuration $(\pi g_{7/2}\pi d_{5/2})^2(\pi h_{11/2})^2$ are too high in energy as compared to the data (except for 16^+, which agrees with experiment). On the other hand, the energies calculated with the neutron core-excited configurations can describe the data much better. This indicates that the inclusion of neutron core-excited configurations is indispensable in shell-model calculations for these $N = 82$ isotones. Among the two neutron core-excited configurations, the energy levels calculated with $(\pi g_{7/2}\pi d_{5/2})^4(\nu h_{11/2})^{-1}(\nu f_{7/2})^1$ generally agree with the data. But for the 10^+ and 16^+ states, those of the
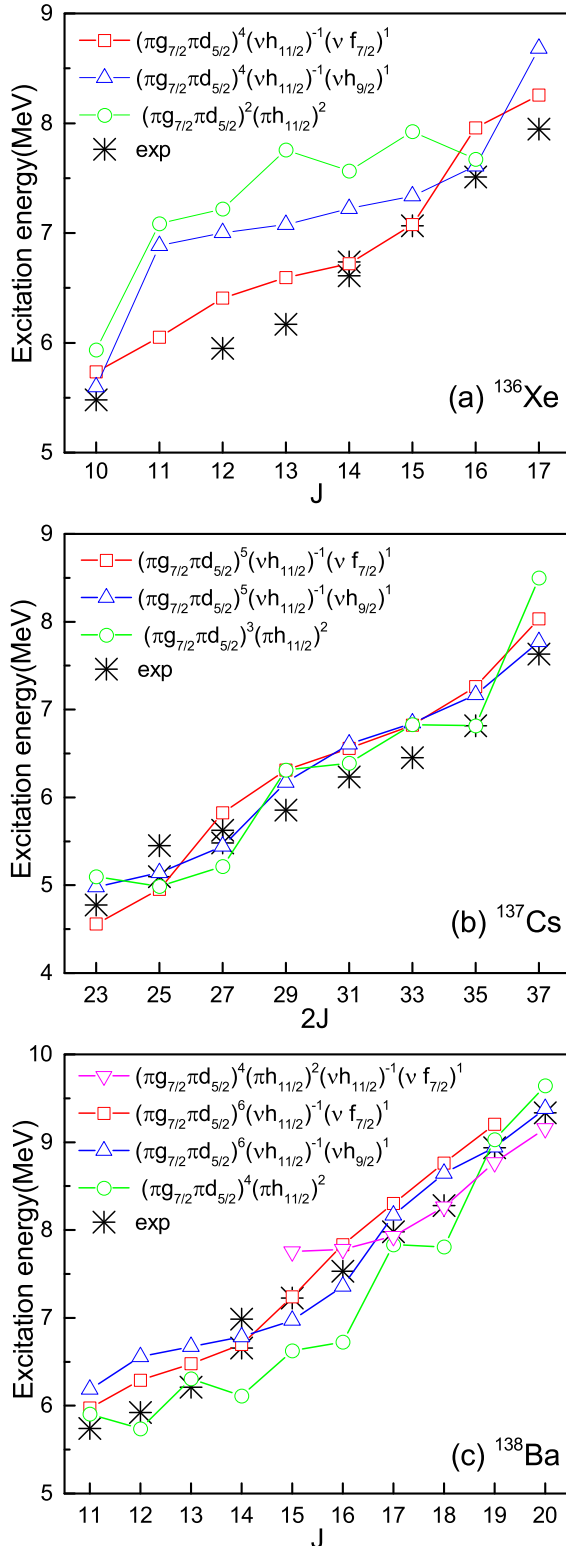
FIG. 3. The theoretical lowest excitation energies as a function of spin for the high-spin positive-parity states corresponding to a leading configuration in the $N = 82$ isotones ^{136}Xe (a), ^{137}Cs (b), and ^{138}Ba (c). The observed experimental data [32] are drawn with asterisks for comparison.

$(\pi g_{7/2}\pi d_{5/2})^4(\nu h_{11/2})^{-1}(\nu h_{9/2})^1$ configuration are lower in energy and describe the data better.

For the odd-mass isotone ^{137}Cs, the experimental high-spin states above 4 MeV starting from $(19/2_3^+)$ are well reproduced by the calculation [see Fig. 1(b)]. Unlike the even-even isotone ^{136}Xe, the high-spin structure of ^{137}Cs is much more complicated. As plotted in Fig. 1(b), the calculated $19/2_3^+$ and $21/2_2^+$ states belong to the $(\pi g_{7/2})^3(\pi d_{5/2})^2$ multiplet. The $25/2_2^+$, $27/2_1^+$, $31/2_1^+$, and $35/2_1^+$ states have a predominant component with two-proton excitation to the upper $h_{11/2}$ orbit, forming the $(\pi g_{7/2}\pi d_{5/2})^3(\pi h_{11/2})^2$ configuration. For the rest six states in Fig. 1(b), $23/2_2^+$, $25/2_1^+$, $27/2_2^+$, $29/2_1^+$, $33/2_1^+$, and $37/2_1^+$, our calculation suggests the configuration of neutron core excitations. Among them, $23/2_2^+$, $25/2_1^+$ and $33/2_1^+$ have a leading $(\pi g_{7/2}\pi d_{5/2})^5(\nu h_{11/2})^{-1}(\nu f_{7/2})^1$ configuration while the other three have $(\pi g_{7/2}\pi d_{5/2})^5(\nu h_{11/2})^{-1}(\nu h_{9/2})^1$. The occupation numbers for these states are shown in Fig. 2(b).

We are aware that the above configuration assignments may contain uncertainties as in this nucleus, states built by two-proton excitations to the $\pi h_{11/2}$ orbit and neutron core excitations are very close in energy. In Fig. 3(b), we show the calculated energies of three configurations, all which may contribute to form the discussed high-spin states in ^{137}Cs. It can be seen that the states with two-proton excitations are bundled together with those of neutron core-excited configuration. This is quite different from what we have seen in ^{136}Xe [Fig. 3(a)]. This may cause ambiguities when configurations are assigned to the high-spin states of ^{137}Cs in Fig. 1(b). In Ref. [32], a band in ^{137}Cs with band-head spin $(25/2_2^+)$ has been detected above 5.452 MeV (see band (d) in Fig. 1 of Ref. [32]). It could correspond to one of these three excitation configurations shown in Fig. 3(b), or could have a mixed structure from them. For the observed band (c) between 4.350 and 5.481 Mev (see Fig. 1 of Ref. [32]), the authors speculated that neutron core excitation should be considered. According to our calculation, this band also has a mixed structure.

We present in Fig. 1(c) the results for high-spin positive-parity states above 5 MeV in ^{138}Ba. For this isotone, the calculation compares with the experimental levels qualitatively. The predicted 11_1^+ state lies below the 12_1^+ state while a reversed order is suggested by experiment. The obtained level spacings of the calculated states between 11_1^+ and 18_1^+ (roughly from 5 to 8 MeV of excitation) show differences from the observation. Nevertheless, the two highest-spin states (19_1^+) and (20_1^+) around 9 MeV in excitation are correctly reproduced. From the occupation numbers shown in Fig. 2(c), we find that most of the high-spin positive-parity states, except 11_1^+, 19_1^+, and 20_1^+, are due to the two-proton excitation to the $\pi h_{11/2}$ orbit with the $(\pi g_{7/2}\pi d_{5/2})^4(\pi h_{11/2})^2$ configuration. The 11_1^+ state has mainly the $(\pi g_{7/2})^4(\pi d_{5/2})^2$ configuration. The 19_1^+ and 20_1^+ states belong to the $(\pi g_{7/2}\pi d_{5/2})^4(\pi h_{11/2})^2$ $(\nu h_{11/2})^{-1}(\nu f_{7/2})^1$ multiplet. This latter configuration contributes to the creation of the largest angular momentum states in the study. Obviously, the high-spin structure of ^{138}Ba are qualitatively different from that of ^{136}Xe or ^{137}Cs.

To further discuss the high-spin structure in ^{138}Ba, the calculated energies for the 11^+ to 20^+ states from four configurations are drawn in Fig. 3(c). As one can see,

among the four different configurations, those belonging to $(\pi g_{7/2} \pi d_{5/2})^4 (\pi h_{11/2})^2$ are the lowest (except for the highest spin states 19^+ and 20^+), which favors the two-proton excitation to the $\pi h_{11/2}$ orbit. Two regular γ-ray cascades were observed in the high-spin states of ^{138}Ba (see Fig. 7 of Ref. [32]). One consists of four states from (11_1^+) to (14_1^+), and the other has a band-head spin (14_2^+) at 6.987 MeV. As seen in Fig. 3(c), these two bands must belong to different structures. The one with the $(\pi g_{7/2} \pi d_{5/2})^4 (\pi h_{11/2})^2$ configuration exhibits staggerings with spin, which well describes the experimental (12_2^+) and (13_1^+) states. From $J = 14$ to 18, the neutron core-excited configurations can better describe the data. Two such configurations from the calculation, $(\pi g_{7/2} \pi d_{5/2})^6 (\nu h_{11/2})^{-1} (\nu f_{7/2})^1$ and $(\pi g_{7/2} \pi d_{5/2})^6 (\nu h_{11/2})^{-1} (\nu h_{9/2})^1$, coincide at $J = 14$. In fact, two closely lying $J = 14$ states have been observed experimentally. Above $J = 14$, the calculated energy levels with the neutron core-excited configurations can well describe the trend of the observation. In addition, the $(\pi g_{7/2} \pi d_{5/2})^4 (\pi h_{11/2})^2 (\nu h_{11/2})^{-1} (\nu f_{7/2})^1$ configuration can well describe the highest spin states from $J = 17$ to 20, as seen in Fig. 3(c). We note that the calculated yrast states from 12^+ to 18^+ with the $(\pi g_{7/2} \pi d_{5/2})^4 (\pi h_{11/2})^2$ configuration by the empirical interaction has the similar staggering trend as in our calculation (see Fig. 14(b) of Ref. [32]).

B. Negative-parity states

The main structure of negative-parity states in the $N = 82$ isotones above ^{132}Sn is simply built by removing one proton from the gd shell to the $h_{11/2}$ orbit. This leads to $(\pi g_{7/2} \pi d_{5/2})^{n-1} (\pi h_{11/2})^1$ as the lowest negative-parity configuration. As one can see in Figs. 1(a)–1(c), the adopted EPQQM interaction reproduces well the experimental negative-parity states in ^{136}Xe, ^{137}Cs, and ^{138}Ba, both in excitation energies and their orders.

In Fig. 1(a), we confirm that the observed (9_1^-), (11_1^-), (13_1^-), and (14_1^-) states in ^{136}Xe correspond to the calculated 9_1^-, 11_1^-, 13_1^-, and 14_1^- ones. In addition, we predict a 10_1^- and a 12_1^- state, which are degenerate with the 11_1^- and 13_1^- states, respectively, and locate just above the respective ones. The calculation shows that the states from 9_1^- to 13_1^- all are members of the $(\pi g_{7/2})^3 (\pi h_{11/2})^1$ multiplet. Only the highest one, the 14_1^- state, has a pure $(\pi g_{7/2})^2 (\pi d_{5/2})^1 (\pi h_{11/2})^1$ configuration.

Similarly, the group of observed high-spin negative-parity states from $(19/2^-)$ to $(31/2^-)$ in ^{137}Cs [see Fig. 1(b)] correspond to the calculated yrast states for these angular momenta. We predict a $25/2_1^-$ state which is nearly degenerate with the known $27/2_1^-$ one. The calculation suggests that the states from $19/2_1^-$ to $27/2_1^-$ all have a leading configuration of $(\pi g_{7/2})^4 (\pi h_{11/2})^1$, and the highest $29/2_1^-$ and $31/2_1^-$ ones belong to the $(\pi g_{7/2})^3 (\pi d_{5/2})^1 (\pi h_{11/2})^1$ multiplet.

For ^{138}Ba, with the reasonably good agreement between theory and experiment, the tentatively assigned spin and parity for the negative-parity states shown in Fig. 1(c) are confirmed by the calculation. The missing 10_1^- state is predicted to be between 9_1^- and 11_1^- near 4 MeV. Moreover, the missing 12_1^- state is predicted to be degenerate with 13_1^-. The

analysis of the wave functions indicates that the states from 9_1^- to 13_1^- are mainly due to one-proton excitation from the $\pi g_{7/2}$ orbit to $\pi h_{11/2}$, with the predominant configuration of $(\pi g_{7/2})^5 (\pi h_{11/2})^1$, while the 13_2^-, 14_1^-, and 15_1^- states have the main configuration of $(\pi g_{7/2})^4 (\pi d_{5/2})^1 (\pi h_{11/2})^1$. Interestingly, our calculation indicates that the observed 16_1^- and 17_1^- states have a neutron core-excited structure. These two states are calculated to have the leading configuration of $(\pi g_{7/2} \pi d_{5/2})^5 (\pi h_{11/2})^1 (\nu h_{11/2})^{-1} (\nu f_{7/2})^1$. However, the configuration of neutron core excitations from the $\nu d_{3/2}$ orbit does not show up in the negative-parity states in ^{138}Ba, which was experimentally observed in the lighter $N = 82$ isotones ^{134}Te and ^{135}I [29] and confirmed by our previous shell-model calculation [34].

In Figs. 1(a) and 1(b), we also predict some negative-parity states built by neutron core excitations in ^{136}Xe and ^{137}Cs. The predicted 15_1^-, 16_1^- states in ^{136}Xe and the $33/2_1^-$, $35/2_1^-$ states in ^{137}Cs at excitation energies of 7.348, 7.486, 6.610, and 6.890 MeV, respectively, are examples of these, which have the leading configurations of $(\pi g_{7/2} \pi d_{5/2})^{n-1} (\pi h_{11/2})^1 (\nu h_{11/2})^{-1} (\nu f_{7/2})^1$.

When we discuss negative-parity states, let us comment on the spurious center-of-mass motion in the 1^- states. The center-of-mass problem concerns momentum conservation associated with the translational invariance required in the nuclear wave function. Since excited nuclear states should correspond to excitation of the internal degrees of freedom only, the center-of-mass excitation should be eliminated. The problem was investigated early by Elliott and Skyrme [53] in their first cross-shell-excitation calculation for ^{16}O in the complete p- and sd-shell model space, with $0p$ orbit below and the $1s$ and $0d$ orbits above the $N = 8$ shell gap. Note in this light mass region, the dominant components in the negative-parity wave functions are the coupling of a $0p$ hole with either a $1s$ or a $0d$ particle. It was shown later [54,55] that the low-lying 1^- spuriosities contaminate the wave functions, and a careful removal of them is necessary. However, in the general case, the problem is very complex, and therefore an exact separation of the spurious components is often hardly possible.

In the present calculation, we do not introduce a procedure that explicitly eliminates low-lying 1^- spuriosities, although in principle these can exist in our states with the coupling of the neutron $1d_{3/2}$ with $2p_{1/2}$ or $2p_{3/2}$. We argue that for heavy nuclei discussed in this paper, the spurious center-of-mass problem can practically be neglected. In Ref. [56], a general discussion was given that such spuriosities have an effect of the order $1/A$, with A being the mass number. This means that in the worst case, our calculated energies in Fig. 1 may only have a $\approx 0.7\%$ shift by the spuriosities, but even this does not happen in our calculation. We have checked the occupation numbers for all the states in Fig. 1 and confirmed that the occupation numbers of $\nu d_{3/2}$ orbit for all the calculated states, not only the low-lying states but also the high-spin ones with both parities, are exactly 4 for the $N = 82$ isotones. This indicates that in our calculation, no neutrons from $\nu d_{3/2}$ are cross-shell excited. We also checked that due to the existence of many other higher-j single-particle levels in heavy nuclei, the occupations in the upper $\nu 2p_{3/2}$ and $\nu 2p_{1/2}$ orbits in the present calculation are negligibly small. This is distinguished

with the light nuclei such as ^{16}O where only the upper 1s and 0d orbits are the components in the wave functions.

C. Analysis of ESPEs

The isotonically dependent structure in the high-spin states of the three $N = 82$ isotones deserves further discussion. We have shown that the two excitation modes, the neutron core excitation across the $N = 82$ shell gap and the two-proton excitation to the $h_{11/2}$ orbit, compete with each other in the same energy range. The competition is clearly visualized in Fig. 3. For example, in ^{136}Xe, the energies of the neutron core-excited configuration are generally lower than those of the two-proton excitation to the $\pi h_{11/2}$ orbit, while in ^{137}Cs with only one more proton than ^{136}Xe, the energies of the two modes become compatible throughout the entire spin range. Going up to the heavier ^{138}Ba isotone with two more protons as compared to ^{136}Xe, the energies of the configurations with two-proton excitations are the lowest (except for the highest spin states). In addition, the competition between the neutron core excitations to the $\nu f_{7/2}$ and to the $\nu h_{9/2}$ orbit are also evident. All these seem to suggest a rapid shell evolution along the $N = 82$ line. Shell evolution in exotic mass regions may be governed by the monopole interactions originating from the tensor force, as discussed by Otsuka *et al.* [47].

In order to understand the structural evolution in the $N = 82$ isotones above ^{132}Sn, we study the proton and neutron ESPEs under the influence of the monopole corrections. As introduced in Sec. II, Eq. (2) suggests explicitly that the monopole corrections can affect the occupation of valence nucleons on certain orbits. In the present work, we have two relevant monopole corrections terms, $k_{mc}(\pi g_{7/2}, \pi h_{11/2})$ and $k_{mc}(\pi g_{7/2}, \nu h_{9/2})$, which can lead to variations in the ESPEs of the $N = 82$ isotones with different valence proton numbers. In Fig. 4, we plot the calculated ESPEs, with the proton number Z varying from 50 to 58, for the relevant proton and neutron orbits for the $N = 82$ isotones. In Fig. 4(a), the proton ESPEs for the $\pi g_{7/2}$, $\pi d_{5/2}$, $\pi s_{1/2}$, and $\pi d_{3/2}$ orbits show moderate increase with increasing Z. In a sharp contrast, that for the $\pi h_{11/2}$ orbit decreases rapidly. This is because that, as the present interaction employs an attractive monopole correction, $k_{mc}(\pi g_{7/2}, \pi h_{11/2}) = -0.15$ MeV [34], the $\pi h_{11/2}$ orbit is lowered significantly with the enhancement of proton's occupation on the $\pi g_{7/2}$ orbit. As a result, for the heavy $N = 82$ isotones, protons are easily excited to the $\pi h_{11/2}$ orbit. In Fig. 4(b), one sees that the calculated neutron ESPEs are almost constant for different Z's, except for $\nu h_{9/2}$. This happens because of the other attractive monopole correction, $k_{mc}(\pi g_{7/2}, \nu h_{9/2}) = -0.6$ MeV [34]. Because of this monopole term, the $\nu h_{9/2}$ orbit intrudes rapidly into the lower lying orbits as Z increases. The decreasing $\nu h_{9/2}$ energy causes effectively a quenching of the neutron $N = 82$ shell gap for larger Z systems, which makes excitations across the shell gap easier.

Without complicated numerical calculation as presented above, the competing picture of the two high-spin excitation modes can be clearly seen by estimating the excitation energies of two-proton excitation to the $\pi h_{11/2}$ orbit and those of the neutron core excitation across the $N = 82$
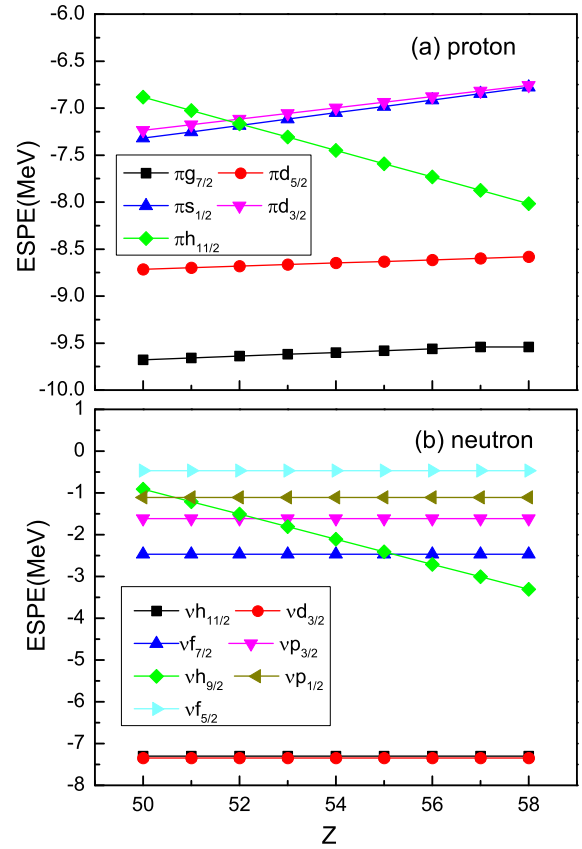

FIG. 4. Effective single-particle energies (ESPEs) calculated by the EPQQM model for proton (a) and neutron (b) orbits of the $N = 82$ isotones beyond ^{132}Sn.

closed shell. The estimate considers the quasiparticles' excitation based on the BCS theory [56]. The BCS quasiparticle energy for protons and neutrons can be obtained from $E_{ik} = \sqrt{(\varepsilon_{ik} - \lambda_i)^2 + \Delta_i^2}$, where $i = \pi$ or ν, ε_{ik} is the energy of the kth single-particle state, λ_i is the Fermi energy, and Δ_i is the pairing gap. For a given isotone, we use the ESPE of the corresponding valence orbit for ε_{ik} and take the empirical values of Δ_i for the $N = 82$ isotones (see below). Only λ_i needs to be determined by solving the equation for the valence-particle number, $N_i = \sum_{k>0}\{1 - (\varepsilon_{ik} - \lambda_i)/[(\varepsilon_{ik} - \lambda_i)^2 + \Delta_i^2]^{1/2}\}$. We then compare the energies of relevant configurations $(\pi g_{7/2})^{n-2}(\pi h_{11/2})^2$, $(\pi g_{7/2})^n(\nu h_{11/2})^{-1}(\nu f_{7/2})^1$, and $(\pi g_{7/2})^n(\nu h_{11/2})^{-1}(\nu h_{9/2})^1$, and denote them respectively as E_{2p}, E_{1n}, and E'_{1n} in the following discussion. As the proton-coupling configuration involves two-particle–two-hole (2p2h) excitation, four-proton quasiparticles' excitation energy is calculated for E_{2p}. For the neutron core-excited configuration, two neutron quasiparticles' excitation energy is considered as E_{1n} and E'_{1n} because this is one-particle–one-hole (1p1h) excitation.

We set the proton pairing gap $\Delta_\pi = 0.94$ MeV, which is evaluated from the two-parameter phenomenological formula c/A^α ($c = 4.31$ MeV, $\alpha = 0.31$) reported in Ref. [57]. Owing to the $N = 82$ closed shell, the neutron paring gap $\Delta_\nu = 1.98$ MeV is estimated from the arithmetic mean value of experimental data [52] through the $N = 82$ isotonic chain
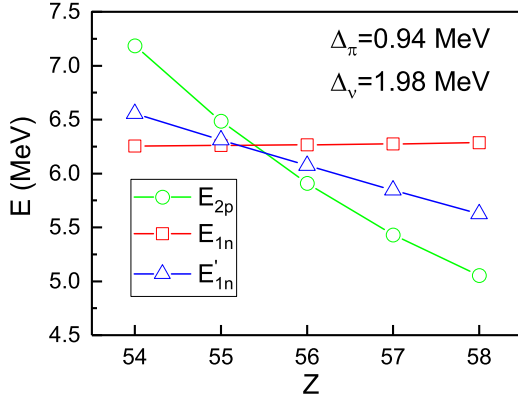
FIG. 5. The values of E_{2p}, E_{1n}, and E'_{1n} as functions of proton number Z for the $N = 82$ isotones.

from $A = 131$ to 140. Those experimental pairing gaps are measured by the so-called three-point formula [52,58] defined by the binding energy difference. In Fig. 5, the so-calculated E_{2p}, E_{1n}, and E'_{1n} are shown as functions of proton number Z for the $N = 82$ isotones. With increasing Z, it can be seen that E_{2p} and E'_{1n} decrease gradually, while E_{1n} essentially keeps constant. For $Z = 54$, E_{1n} and E'_{1n} are lower in energy than E_{2p} by about 1 MeV, and therefore the neutron core excitation across the $N = 82$ closed shell is the preferred mode. As Z increases, E_{2p} goes down to approach E_{1n} and E'_{1n}, and finally becomes the lowest for $Z = 56$ and beyond. For heavier $N = 82$ isotones with even larger Z's, the mode of two-proton excitation to the $\pi h_{11/2}$ orbit clearly wins in the competition. This result indicates that the neutron core excitation should be easier for the lighter $N = 82$ isotones with $Z \leqslant 54$, while the two-proton excitation to the $\pi h_{11/2}$ orbit is the preferred mode for those with $Z \geqslant 57$. For the isotones with $Z = 55$ and 56, the two kinds of configurations compete in close energy ranges, and the two excitation modes may thus coexist. One also sees the competition between the neutron core excitations to the $\nu f_{7/2}$ and to the $\nu h_{9/2}$ orbits: For $Z = 54$ and 55, E'_{1n} is a little higher than E_{1n}, but for $Z \geqslant 56$, E'_{1n} becomes lower. The above estimate illustrates clearly the structural evolution found with the realistic calculation in Fig. 3.

IV. CONCLUSIONS

Motivated by the recent experimental data [32], we have applied the EPQQM interaction developed in our previous work [34] to describe the high-spin states in the heavier $N = 82$ isotones ^{136}Xe, ^{137}Cs, and ^{138}Ba. With a considerably large model space containing neutron core-excitation configurations across the $N = 82$ shell gap, we have reproduced the experimental levels of these three isotones for both the low-lying and high-spin states. For the low-lying positive-parity states, we have discussed the configurations of the yrast states, which are consistent with the results of other shell-model calculations [32,33]. We have also compared our calculated $B(E2)$ values with the available data.

The main discussion focus of the present article is the structure of the positive-parity high-spin states. Our calculations have explored clear differences in the high-spin

structure in the three $N = 82$ isotones. We have found that many of the high-spin states observed in ^{136}Xe have the main configurations of neutron core excitations across the $N = 82$ shell gap. In contrast to ^{136}Xe, only some high-spin states in ^{137}Cs contain the neutron core-excited components. The other high-spin states are explained with the configuration of two-proton excitation to the $\pi h_{11/2}$ orbit. However, such two-proton excitations become predominant in most of the calculated high-spin states in ^{138}Ba. Our calculations have also reproduced the observed negative-parity states in these three isotones. In addition, we have predicted some neutron core-excited states in ^{138}Ba. For example, the 19^+_1 and 20^+_1 states of ^{138}Ba could have the configuration of $(\pi g_{7/2}\pi d_{5/2})^4(\pi h_{11/2})^2(\nu h_{11/2})^{-1}(\nu f_{7/2})^1$. The 16^-_1 and 17^-_1 states could be the members of the $(\pi g_{7/2}\pi d_{5/2})^5(\pi h_{11/2})^1(\nu h_{11/2})^{-1}(\nu f_{7/2})^1$ multiplet.

Thus, a picture of competition between two kinds of excitation modes, namely the neutron core excitation across of the $N = 82$ shell gap and two-proton excitation to the $\pi h_{11/2}$ orbit, has been established for the high-spin states in these $N = 82$ isotones. This picture has been reinforced by analyzing the theoretical ESPEs. We have shown that for the $N = 82$ isotones beyond ^{132}Sn, the monopole effect related to the proton $g_{7/2}$ orbit influences strongly the variation of ESPEs, leading to the structural evolution along the $N = 82$ isotonic line. In particular, the two monopole correction terms adopted in our EPQQM interaction, $k_{mc}(\pi g_{7/2}, \pi h_{11/2})$ and $k_{mc}(\pi g_{7/2}, \nu h_{9/2})$, play important roles. We have found that both the neutron core-excited configurations $(\nu h_{11/2})^{-1}(\nu f_{7/2})^1$ and $(\nu h_{11/2})^{-1}(\nu h_{9/2})^1$ can be dominant in the high-spin positive-parity states of these $N = 82$ isotones, which are caused by the attractive monopole correction $k_{mc}(\pi g_{7/2}, \nu h_{9/2})$. On the other hand, the energies of two-proton excitations to the $\pi h_{11/2}$ orbit depend strongly on the monopole correction $k_{mc}(\pi g_{7/2}, \pi h_{11/2})$.

The present work, together with our previous ones [19,20,34–37], suggests that the neutron core excitation across the $N = 82$ closed shell is important in the structure description of the ^{132}Sn mass region. The monopole corrections play important roles in the discussion. Presently, the monopole correction terms are added into the Hamiltonian in a phenomenological way. Alternative effective interactions that can describe the shell evolution are welcome to describe the heavier $N = 82$ isotones. Recently, an unified realistic interaction [59,60], whose monopole terms are constructed starting from the monopole-based universal force suggested by Otsuka *et al.* [61], has been successfully applied in the shell-model calculations for the pf- and pfg-shell nuclei. Similar application to the ^{132}Sn mass region is in progress.

[1] J. P. Schiffer, S. J. Freeman, J. A. Caggiano, C. Deibel, A. Heinz, C.-L. Jiang, R. Lewis, A. Parikh, P. D. Parker, K. E. Rehm *et al.*, Phys. Rev. Lett. **92**, 162501 (2004); **110**, 169901(E) (2013).

[2] J.-y. Zhang, Y. Sun, M. Guidry, L. L. Riedinger, and G. A. Lalazissis, Phys. Rev. C **58**, R2663 (1998).

[3] K. L. Jones, A. S. Adekola, D. W. Bardayan, J. C. Blackmon, K. Y. Chae, K. A. Chipps, J. A. Cizewski, L. Erikson, C. Harlin, R. Hatarik *et al.*, Nature (London) **465**, 454 (2010).

[4] J. M. Allmond, A. E.Stuchbery, J. R. Beene, A.Galindo-Uribarri, J. F. Liang, E. Padilla-Rodal, D. C. Radford, R. L. Varner, A. Ayres, J. C. Batchelder *et al.*, Phys. Rev. Lett. **112**, 172701 (2014).

[5] D. T. Yordanov, D. L. Balabanski, J. Bieroń, M. L. Bissell, K. Blaum, I. Budinčević, S. Fritzsche, N. Frömmgen, G. Georgiev, Ch. Geppert *et al.*, Phys. Rev. Lett. **110**, 192501 (2013).

[6] G. S. Simpson, G. Gey, A. Jungclaus, J. Taprogge, S. Nishimura, K. Sieja, P. Doornenbal, G. Lorusso, P.-A. Söderström, T. Sumikama *et al.*, Phys. Rev. Lett. **113**, 132502 (2014).

[7] J. M. Allmond, A. E. Stuchbery, C. Baktash, A. Gargano, A. Galindo-Uribarri, D. C. Radford, C. R. Bingham, B. A. Brown, L. Coraggio, A. Covello *et al.*, Phys. Rev. Lett. **118**, 092503 (2017).

[8] J. Hakala, J. Dobaczewski, D. Gorelov, T. Eronen, A. Jokinen, A. Kankainen, V. S. Kolhinen, M. Kortelainen, I. D. Moore, H. Penttilä *et al.*, Phys. Rev. Lett. **109**, 032501 (2012).

[9] H. Watanabe, G. Lorusso, S. Nishimura, Z. Y. Xu, T. Sumikama, P.-A. Söderström, P. Doornenbal, F. Browne, G. Gey, H. S. Jung *et al.*, Phys. Rev. Lett. **111**, 152501 (2013).

[10] H. Watanabe, G. Lorusso, S. Nishimura, T. Otsuka, K. Ogawa, Z. Y. Xu, T. Sumikama, P.-A. Söderström, P. Doornenbal, Z. Li *et al.*, Phys. Rev. Lett. **113**, 042502 (2014).

[11] J. Taprogge, A. Jungclaus, H. Grawe, S. Nishimura, P. Doornenbal, G. Lorusso, G. S. Simpson, P.-A. Söderström, T. Sumikama, Z. Y. Xu *et al.*, Phys. Rev. Lett. **112**, 132501 (2014).

[12] R. L. Kozub, G. Arbanas, A. S. Adekola, D. W. Bardayan, J. C. Blackmon, K. Y. Chae, K. A. Chipps, J. A. Cizewski, L. Erikson, R. Hatarik *et al.*, Phys. Rev. Lett. **109**, 172501 (2012).

[13] J. Van Schelt, D. Lascar, G. Savard, J. A. Clark, P. F. Bertone, S. Caldwell, A. Chaudhuri, A. F. Levand, G. Li, G. E. Morgan *et al.*, Phys. Rev. Lett. **111**, 061102 (2013).

[14] G. Lorusso, S. Nishimura, Z. Y. Xu, A. Jungclaus, Y. Shimizu, G. S. Simpson, P.-A. Söderström, H. Watanabe, F. Browne, P. Doornenbal *et al.*, Phys. Rev. Lett. **114**, 192501 (2015).

[15] D. Atanasov, P. Ascher, K. Blaum, R. B. Cakirli, T. E. Cocolios, S. George, S. Goriely, F. Herfurth, H.-T. Janka, O. Just *et al.*, Phys. Rev. Lett. **115**, 232501 (2015).

[16] V. Vaquero, A. Jungclaus, P. Doornenbal, K. Wimmer, A. Gargano, J. A. Tostevin, S. Chen, E. Nácher, E. Sahin, Y. Shiga *et al.*, Phys. Rev. Lett. **118**, 202502 (2017).

[17] A. Jungclaus, L. Cáceres, M. Górska, M. Pfützner, S. Pietri, E. Werner-Malento, H. Grawe, K. Langanke, G. Martínez-Pinedo, F. Nowacki *et al.*, Phys. Rev. Lett. **99**, 132501 (2007).

[18] M. Górska, L. Cáceres, H. Grawe, M. Pfützner, A. Jungclaus, S. Pietri, E. Werner-Malento, Z. Podolyák, P. H. Regan, D. Rudolph *et al.*, Phys. Lett. B **672**, 313 (2009).

[19] H.-K. Wang, K. Kaneko, and Y. Sun, Phys. Rev. C **89**, 064311 (2014).

[20] H.-K. Wang, K. Kaneko, and Y. Sun, Phys. Rev. C **91**, 021303(R) (2015).

[21] J. B. Albert, G. Anton, I. Badhrees, P. S. Barbeau, R. Bayerlein, D. Beck, V. Belov, M. Breidenbach, T. Brunner, G. F. Cao *et al.*, Phys. Rev. Lett. **120**, 072701 (2018).

[22] E. E. Peters, T. J. Ross, S. H. Liu, M. T. McEllistrem, and S. W. Yates, Phys. Rev. C **95**, 014325 (2017).

[23] E. E. Peters, T. J. Ross, B. P. Crider, and S. W. Yates, Euro. Phys. J. Web-Conf. **178**, 02028 (2018).

[24] P. J. Daly, P. Bhattacharyya, C. T. Zhang, Z. W. Grabowski, R. Broda, B. Fornal, I. Ahmad, T. Lauritsen, L. R. Morss, W. Urban *et al.*, Phys. Rev. C **59**, 3066 (1999).

[25] R. Broda, B. Fornal, P. J. Daly, C. T. Zhang, P. Bhattacharyya, Z. W. Grabowski, J. F. C. Cocks, P. A. Butler, P. T. Greenlees, G. D. Jones *et al.*, Phys. Rev. C **59**, 3071 (1999).

[26] C. T. Zhang, P. Bhattacharyya, P. J. Daly, R. Broda, Z. W. Grabowski, D. Nisius, I. Ahmad, T. Ishii, M. P. Carpenter, L. R. Morss *et al.*, Phys. Rev. Lett. **77**, 3743 (1996).

[27] W. Urban, W. Kurcewicz, A. Korgul, P. J. Daly, P. Bhattacharyya, C. T. Zhang, J. L. Durell, M. J. Leddy, M. A. Jones, W. R. Phillips *et al.*, Phys. Rev. C **62**, 027301 (2000).

[28] B. Fornal, R. Broda, P. J. Daly, P. Bhattacharyya, C. T. Zhang, Z. W. Grabowski, I. Ahmad, D. Seweryniak, I. Wiedenhöver, M. P. Carpenter *et al.*, Phys. Rev. C **63**, 024322 (2001).

[29] S. K. Saha, C. Constantinescu, P. J. Daly, P. Bhattacharyya, C. T. Zhang, Z. W. Grabowski, B. Fornal, R. Broda, I. Ahmad, D. Seweryniak *et al.*, Phys. Rev. C **65**, 017302 (2001).

[30] K. Li, Y. X. Luo, J. K. Hwang, A. V. Ramayya, J. H. Hamilton, S. J. Zhu, C. Goodin, H. L. Crowell, J. O. Rasmussen, I. Y. Lee *et al.*, Phys. Rev. C **75**, 044314 (2007).

[31] W. Reviol, D. G. Sarantites, J. M. Elson, J. E. Kinnison, A. Gargano, S. Bottoni, R. V. F. Janssens, J. M. Allmond, A. D. Ayangeakaa, M. P. Carpenter *et al.*, Phys. Rev. C **94**, 034309 (2016).

[32] A. Astier, M.-G. Porquet, Ts. Venkova, D. Verney, Ch. Theisen, G. Duchêne, F. Azaiez, G. Barreau, D. Curien, I. Deloncle *et al.*, Phys. Rev. C **85**, 064316 (2012).

[33] P. C. Srivastava, M. J. Ermamatov, and I. O. Morales, J. Phys. G **40**, 035106 (2013).

[34] H. Jin, M. Hasegawa, S. Tazaki, K. Kaneko, and Y. Sun, Phys. Rev. C **84**, 044324 (2011).

[35] H.-K. Wang, Y. Sun, H. Jin, K. Kaneko, and S. Tazaki, Phys. Rev. C **88**, 054310 (2013).

[36] H.-K. Wang, K. Kaneko, Y. Sun, Y.-Q. He, S.-F. Li, and J. Li, Phys. Rev. C **95**, 011304(R) (2017).

[37] H.-K. Wang, S. K. Ghorui, K. Kaneko, Y. Sun, and Z. H. Li, Phys. Rev. C **96**, 054313 (2017).

[38] M. Hasegawa and K. Kaneko, Phys. Rev. C **59**, 1449 (1999).

[39] M. Hasegawa, K. Kaneko, and S. Tazaki, Nucl. Phys. A **674**, 411 (2000).

[40] M. Hasegawa, Y. Sun, S. Tazaki, K. Kaneko, and T. Mizusaki, Phys. Lett. B **696**, 197 (2011).

[41] K. Kaneko, Y. Sun, M. Hasegawa, and T. Mizusaki, Phys. Rev. C **78**, 064312 (2008).

[42] K. Kaneko, Y. Sun, T. Mizusaki, and M. Hasegawa, Phys. Rev. C **83**, 014320 (2011).

[43] L. Coraggio, A. Covello, A. Garganoa, N. Itaco, and T. T. S. Kuo, Prog. Part. Nucl. Phys. **62**, 135 (2009).

[44] J. Blomqvist, Acta Phys. Pol. B **30**, 697 (1999).

[45] W. Rae, NUSHELLX code, http://www.garsington.eclipse.co.uk/

[46] N. A. Smirnova, B. Ballya, K. Heyde, F. Nowacki, and K. Sieja, Phys. Lett. B **686**, 109 (2010).

[47] T. Otsuka, T. Suzuki, R. Fujimoto, H. Grawe, and Y. Akaishi, Phys. Rev. Lett. **95**, 232502 (2005).

[48] H. Naidja, F. Nowacki, and B. Bounthong, Phys. Rev. C **96**, 034312 (2017).

[49] S. Sarkar and M. S. Sarkar, Phys. Rev. C **64**, 014312 (2001).

[50] L. Coraggio, A. Covello, A. Gargano, N. Itaco, and T. T. S. Kuo, Phys. Rev. C **80**, 044320 (2009).

[51] E. Teruya, N. Yoshinaga, K. Higashiyama, and A. Odahara, Phys. Rev. C **92**, 034320 (2015).

[52] http://www.nndc.bnl.gov/nudat2/

[53] J. P. Elliott and T. H. R. Skyrme, Proc. R. Soc. London A **232**, 561 (1955).

[54] D. H. Gloeckner and R. D. Lawson, Phys. Lett. B **53**, 313 (1974).

[55] D. J. Dean, M. T. Ressell, M. Hjorth-Jensen, S. E. Koonin, K. Langanke, and A. P. Zuker, Phys. Rev. C **59**, 2474 (1999).

[56] P. Ring and P. Schuck, *The Nuclear Many-Body Problem* (Spring-Verlag, New York, 1980).

[57] G. F. Bertsch, C. A. Bertulani, W. Nazarewicz, N. Schunck, and M. V. Stoitsov, Phys. Rev. C **79**, 034306 (2009).

[58] W. Satuła, J. Dobaczewski, and W. Nazarewicz, Phys. Rev. Lett. **81**, 3599 (1998).

[59] K. Kaneko, T. Mizusaki, Y. Sun, and S. Tazaki, Phys. Rev. C **89**, 011302(R) (2014).

[60] K. Kaneko, T. Mizusaki, Y. Sun, and S. Tazaki, Phys. Rev. C **92**, 044331 (2015).

[61] T. Otsuka, T. Suzuki, M. Honma, Y. Utsuno, N. Tsunoda, K. Tsukiyama, and M. Hjorth-Jensen, Phys. Rev. Lett. **104**, 012501 (2010).